UNIVERSITY OF CAMBRIDGE
Department of Engineering

Resilient pipes for water distribution and sewer systems

Author Name: Hui Yin Wai (Stephanie)
Supervisor: Dr Sam Stanier
Date: 26/5/2020

I hereby declare that, except where specifically indicated, the work submitted herein is my own original work.

Signed ________________________________ *date* _________26/5/2020_______________

D-SAS229-4: Resilient pipes for water distribution and sewer systems

Stephanie Wai, Robinson College (hyw25)

May 2020

Abstract

With the UK government actively looking to tackle the challenge of leaking pipes, this project aims to focus on studying the importance of cyclic thermal effects and soil-pipe interactions in causing pipe deterioration, and subsequently pipe failure and leakage. The goal of this project is to contribute to the development of a more fundamental understanding of the behaviours of shallowly buried pipeline so as to facilitate resilient pipe network design and to improve the accuracy in identifying pipelines requiring maintenance in the future.

A sensitivity analysis was first carried out to assess the likelihood of thermal expansion force exceeding the threshold for buckling and the axial frictional resistance provided by the soil-pipe interface, hence failing in upheaval buckling or joint failure. It was then discovered that a factor with potentially profound implications in the calculations of stresses around a pipeline, the wedging factor, carries major uncertainty in its form and validity. A simple experiment was subsequently designed to verify the analytical solution of the wedging factor. Due to technical constraints, the experiment could not be completed with a sufficient number of trials. Nonetheless, the experiment pointed out the possibility that the wedging factor function could take another form.

Furthermore, Finite Element Modelling (FEM) was used to better understand the behaviours of shallowly buried pipelines in unsaturated soils. Using an FEM software called Optum, models were built such that the factors of interest, namely soil type, water table, and friction angle, could be varied in turn such that a set of V-H failure envelopes could be obtained. By adopting a Mohr-Coulomb failure criterion, the extra shear strength due to negative pore water pressure in unsaturated soils can be modelled as a cohesion component in the Mohr-

Coulomb failure criterion $(c - \varphi)$. After obtaining V-H failure envelopes from Optum using the $(c - \varphi)$ profiles derived, the V-H failure envelopes were then compared to models proposed in the literature, for example, Tom and White (2019).

There are inadequate existing models for the V-H failure envelopes for shallowly buried pipelines, hence the reason why analytical solutions had to be derived in this Project. After comparing the numerical results to the analytical solution, it was found that the analytical solution derived using an embedded pipe rather than a buried pipe still provided a reasonable approximation for the V-H envelope shape and values. This suggests that there could exist a failure envelope taking a similar form as the model proposed by Tom and White (2019). A possible form of equations giving a reasonable rough fit was also proposed after the analysis. It was also found that the soil-water retention characteristics of using different backfills can have profound implications on the shear strength of the soil stratum, and therefore the designer should thoroughly understand the impact of using a specific backfill and ensure the contractor follows the design accordingly.

In terms of future work, technical difficulties encountered could be easily solved with a longer time frame for the project. For example, it is suggested that the wedging factor test can be repeated easily to give a more representative value when evaluating the stresses and forces acting on and around a buried pipe. Moreover, further numerical analysis can be carried out such that V-H failure envelopes can be derived for shallowly buried pipelines, so as to facilitate easier pipe design and maintenance in the future.

Contents

1. Introduction

1.1 Motivation

It has been estimated that UK water companies on average lost a total amount of 3,170 million litres of water each day (The Daily Mail, 2019). The most apparent implication is that a significant proportion of water supplied never reaches the tap of water users. This becomes a prime concern especially when in warmer months parts of the United Kingdom face drought conditions, therefore making ensuring a sufficient water supply particularly important. Moreover, there can also be other problems caused by leaking pipes or pipe bursts, for example, reduced water pressure in the supply network and hence more power required to raise the water pressure. This means more energy is wasted than ordinarily required, which creates negative environmental implications.

In the process of trying to repair leaking pipe networks, the water companies face a series of technical difficulties preventing them from efficiently reducing leakage in current pipe networks. For example, water companies' representatives have admitted the difficulties range from the millions of potential failure points in an ageing water network, the availability of skilled leakage technicians, to the extreme weather conditions and the stresses caused on existing pipe networks, leakage detection techniques, etc. (Peachey, 2020)

The UK Water Industry Research (UKWIR) has been conducting projects in five separate areas to address the big question of how the industry could achieve zero water leakage by 2020, with the five key areas identified being:

1. The basic mechanisms of bursts and leakage;
2. Leak detection and location methods;
3. Leak repair methods;
4. Leak free new networks; and
5. Water accounting

As pointed out by the UKWIR Report, it is recognised that understanding bursts and leakage, and the underlying mechanisms, is most likely the biggest area to be reviewed (Farrow et al., 2017). Currently, research is heavily focused on better data collection and analysis with the advance in smart meter technologies. However, currently it is still difficult to correctly diagnose the accurate locations of leakages in a pipe network, which in turns suggests that a better understanding of the underlying mechanisms can likely help select the areas that will require more intensive monitoring and check-ups.

1.2 Project Direction

A list of the most probable factors identified that could cause pipe deterioration, which could in turn cause pipe leakage and bursts are:

- Thermal cycles
- Soil-pipe interactions (e.g. shrinkage and swelling of clays)
- Pressure transients
- Soil properties (e.g. soil acidity)
- Installation methods

With the increasing extremes of thermal cycles, it has been suggested that the thermal cycles could exacerbate the deterioration of existing pipe networks of a certain age. Moreover, the research on soil-pipe interactions has only speeded up in recent years, with better numerical models being developed with further advances in finite element modelling. Thus, this project will focus on studying the importance of cyclic thermal effects and soil-pipe interactions in causing pipe deterioration. In short, this project aims to contribute to the development of a more fundamental understanding of buried pipe behaviours so as to facilitate resilient pipe network design in the future.

2. Initial Research and Literature Review

2.1 Definition of Unsaturated Soils

Soil mechanics involves a combination of engineering mechanics and the properties of soils. Soil can be described to consist of a combination of three phases, namely (1) solids, (2) water, and (3) air, where water and air occupies the pores, space that is not occupied by solids in the soil stratum. In simple conventional soil mechanics, a soil is said to be saturated when all pores are filled by water; and it is said to be dry when all pores are filled by air. However, between the two limits, the soil can be described as unsaturated and can behave very differently from a dry soil or a saturated soil.

In terms of saturation ratio, an unsaturated soil can be very roughly defined as a soil where the saturation is between 0 and 1 but neither 0 nor 1, as illustrated by Figure 1.

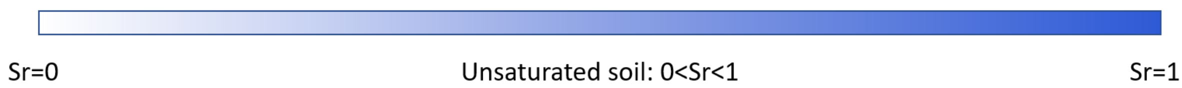

Figure 1. Saturation ratio values of unsaturated soil

The main characteristic of unsaturated soil is that the pore water pressure is usually negative. This is caused by the surface tension of pore water in voids throughout the unsaturated region of the soil. The surface tension creates a suction effect on the surrounding particles, giving the soil matrix “extra strength”. This suction is commonly called matric suction. The surface tension can be explained using a similar phenomenon – capillary rise of water in a capillary tube.

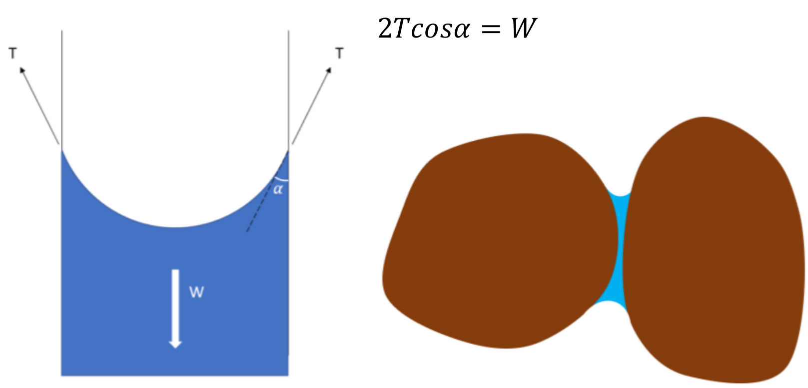

Figure 2. Menisci giving surface tension in the case of capillary tube and between soil particles

In the literature, unsaturated soil is usually better defined than purely using 0<Sr<1 by using different limits. Using the model proposed by Fredlund and Xing (1994), soils can be better sub-divided into three different regions using two different limits in terms of the soil suction values and the respective water content, with the limits being θ_s, the saturated water content, which is the volumetric water content at air entry suction and θ_r, the residual water content, which is the volumetric water content at residual suction. Soils lying in the transition zone are commonly considered as unsaturated soils.

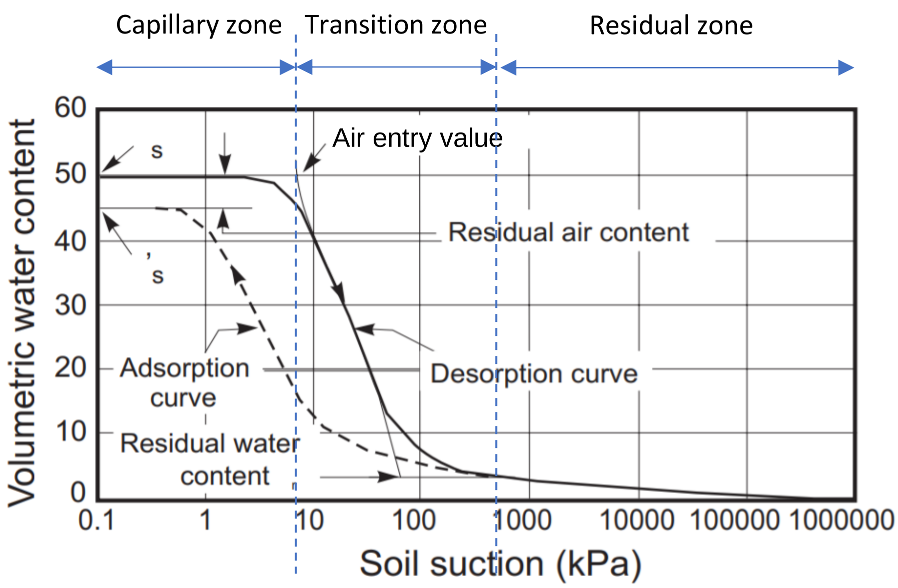

Figure 3. Soil-water characteristic curve defining the three zones by matric suction (Fredlund and Xing, 1994)

The air-entry value (AEV) is the value of matric suction from which air starts to penetrate into the soil matrix. Typically, the finer the soil particles the higher the AEV. The suction at the AEV, air-entry suction, is the suction at which the drying of the soil starts to take place and the soil is said to have entered the transition zone.

Residual suction is when practically no extra moisture is removed from the soil with an increase in the suction applied to the soil matrix. The soil is considered effectively dry.

In the capillary zone, the soil is considered to be saturated. Thus, it is assumed that there is no air present in the pore space. The effective stress of a saturated soil can be expressed using the Terzaghi's equation of effective stresses (1936):

$$\sigma' = \sigma - u_w \quad (2.1)$$

Incorporating equation (2.1) into the Mohr-Coulomb failure criterion:

$$\tau = c' + \sigma' \tan \varphi' \tag{2.2}$$

which can then be substituted into equation (2.2) to give the shear strength of a soil:

$$\tau = c' + \sigma' \tan \varphi' = c' + (\sigma - u_w) \tan \varphi' \tag{2.3}$$

where c' is the effective cohesion and φ' is the internal angle of friction of the soil.

In the residual zone, the soil is considered to be dry. Thus, it is assumed that the effective stress of the soil is the same as the total stress of the soil. The shear strength of a dry soil can be expressed using the Terzaghi's equation of effective stresses:

$$\tau = c' + \sigma' \tan \varphi' = c' + \sigma \tan \varphi' \tag{2.4}$$

In the transition zone, unsaturated soil mechanics apply and the shear strength expression complicates to become a function of saturation ratio, which will be discussed in the following section.

2.2 Shear Strength of Unsaturated Soils

Various models have been proposed to give the shear strength of unsaturated soils. The simple Terzaghi's equation does not apply to unsaturated soils as pore water now only covers a portion of the soil matrix, which means any changes to the effective stresses due to pore water pressure now only acts across a portion of the soil matrix. Thus, the models developed proposed that shear strength of an unsaturated soil is a function of the saturation ratio.

2.2.1 Bishop's model (1959)

In 1959, Bishop pointed out that there are two conditions that the soil matrix must fulfil for Terzaghi's effective stress equation to hold true:

(1) The soil grains are incompressible.

(2) The yield stress in the grain material, which controls the contact area and intergranular shearing resistance, is independent of the confining pressure.

However, actual soils do not fully satisfy these two conditions, which is the reason why Bishop proposed an alternative function, as shown in equation (2.5), to give effective stress in terms of total stress, pore-air pressure and pore-water pressure:

$$\sigma' = (\sigma - u_a) + \chi(u_a - u_w) \tag{2.5}$$

where χ is a soil parameter assumed to be a function of the degree of saturation S_r

Substituting into the Mohr-Coulomb failure criterion gives:

$$\tau = c' + (\sigma - u_a)\tan\varphi' + \chi(u_a - u_w)\tan\varphi' \tag{2.6}$$

However, various literature in the following years attempted to derive a relationship purely between χ and S_r, but to no avail. χ was often found to be heavily dependent on the soil type, and intensive theoretical or experimental efforts were often required to derive χ for an accurate fit between the experimental results and the theoretical values. (Bishop et al, 1960; Bishop and Donald, 1961; Jennings and Burland, 1962) Thus, efforts were made to derive another form of equation to describe effective stresses without the need of such intensive experimental efforts.

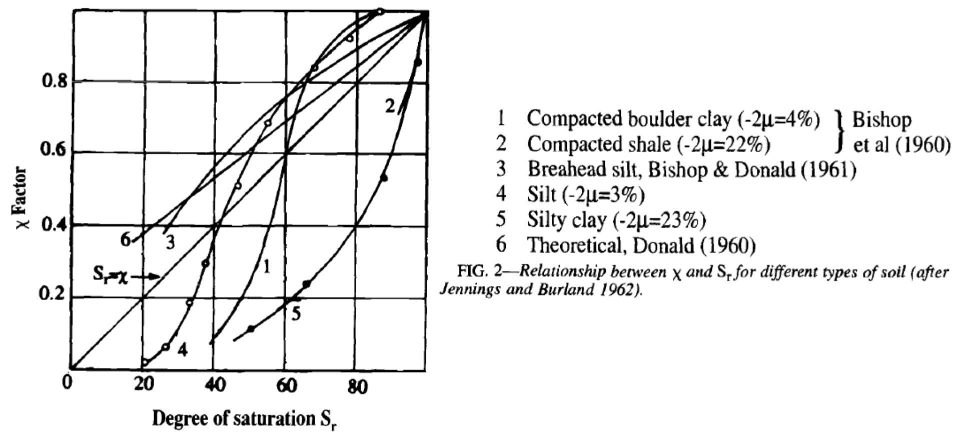

Figure 4. Past attempts to find a fit between χ and S_r. (Öberg and Sällfors, 1997)

2.2.2 Fredlund et al. (1978)

Another approach was adopted by Fredlund et al. (1978). It was proposed that instead of using the χ parameter, two different friction angles φ' and φ^b should be applied to the air entry suction $(\sigma - u_a)$ and matric suction $(u_a - u_w)$ respectively:

$$\tau = c' + (\sigma - u_a)\tan\varphi' + (u_a - u_w)\tan\varphi^b \tag{2.7}$$

However, as φ^b is of a constant value, this model assumed that the shear strength varies proportionately to the matric suction. As seen in Figure 3, this assumption is not true. This assumption was also proved flawed by subsequent literature where the failure envelope was found to be non-linear (Escario and Saez, 1986; Fredlund et al. 1987).

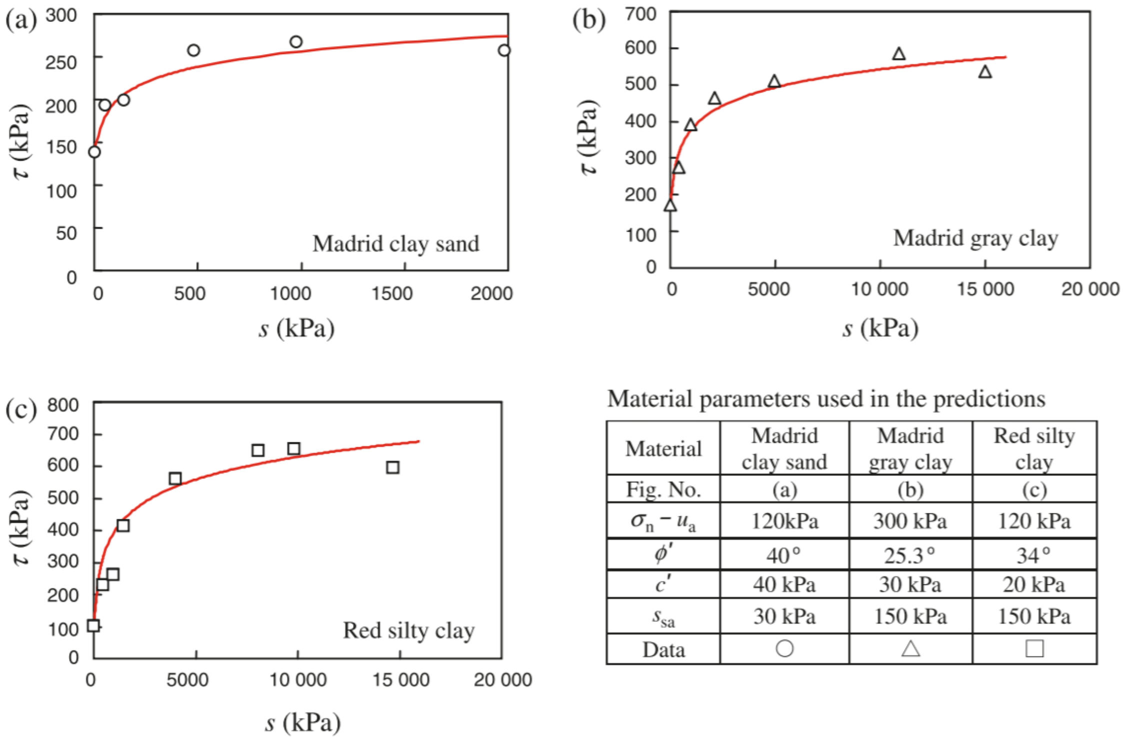

Material	Madrid clay sand	Madrid gray clay	Red silty clay
Fig. No.	(a)	(b)	(c)
$\sigma_n - u_a$	120kPa	300 kPa	120 kPa
φ'	40°	25.3°	34°
c'	40 kPa	30 kPa	20 kPa
s_{sa}	30 kPa	150 kPa	150 kPa
Data	○	△	□

Figure 5. Shear strength versus suction during direct shear tests (Data from Escario and Saez, 1986; Plotted by Zhou and Sheng, 2009)

2.2.3 Öberg and Sällfors (1997)

In order to improve the Bishop's equation such that the χ factor does not require extensive experimental effort, Öberg and Sällfors proposed the hypothesis that χ reflects the fraction of the pore area that is occupied by water. The equation for shear strength is that given by:

$$\tau = c' + \left(\sigma - \frac{A_w}{A_{tot}}u_w - \frac{A_a}{A_{tot}}u_a\right)\tan\varphi' \qquad (2.8)$$

where A_w/A_{tot} = fraction of the pore area occupied by water, and

A_a/A_{tot} = fraction of the pore area occupied by air

However, due to the experimental difficulty in determining the values of the above fractions, Öberg and Sällfors showed that for idealised soils, A_w/A_{tot} and A_a/A_{tot} can be approximated with reasonable accuracy by substituting for S_r and $(1 - S_r)$, as illustrated in Figure 6, the shear strength expression can then be modified as:

$$\tau_f = c' + (\sigma - S_r u_w - (1 - S_r)u_a) tan\, \varphi' \qquad (2.9)$$

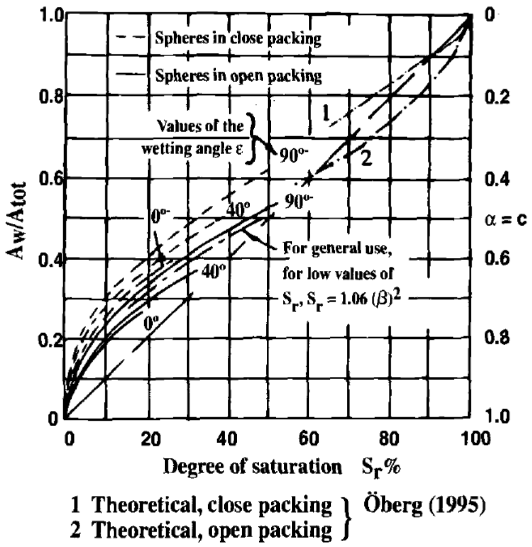

Figure 6. Relationship between A_w/A_{tot} and S_r for idealised solids (Öberg and Sällfors, 1997)

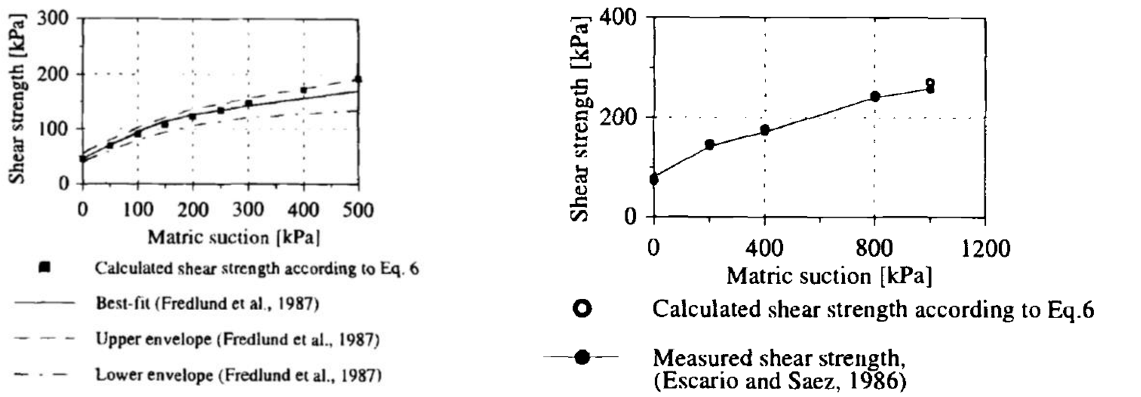

FIG. 12—*Shear strength versus matric suction for the glacial till.* FIG. 15—*Shear strength versus matric suction for the Madrid grey clay.*

Figure 7. Shear strength versus matric suction for glacial till and Madrid grey clay using shear strength values derived in previous literature (Öberg and Sällfors, 1997)

Öberg and Sällfors then proceeded to show that using Equation (2.9), the shear strength calculated lies within the failure envelope as given by Fredlund et al., 1987 experimentally for the glacial till tested. Compared to the results determined by Escario and Saez (1986), it was found that the calculated and measured shear strengths for both the red clay and the grey clay compared well. However, for the Madrid clayey sand, as there was no water retention curve for any material that is similar to the Madrid clayey sand, the shear strengths profiles showed some deviation. Thus, it is equally important to use a representative water retention curve when deriving the values of S_r.

2.3 Soil-Water Characteristics Curves (SWCC)

In order to obtain the correct value of S_r for the application of Equation (2.9) to determine the shear strength of a soil, various soil-water characteristics curves models were developed, with the most commonly used one being the van Genuchten's SWCC (1980). Van Genuchten proposed a relationship between volumetric water content and matric suction such that:

$$S_e = \frac{\theta - \theta_r}{\theta_s - \theta_r} = [1 + (\alpha\psi)^n]^{-m} \tag{2.10}$$

where S_e= effective saturation; ψ = matric suction (kPa) where $\psi = u_a - u_w$(matric suction) ; θ_s = saturated volumetric water content; θ_r = residual volumetric water content; and $\alpha, n\ and\ m$ = empirical fitting parameters and $m = 1 - (1/n)$.

Assuming the soil matrix has a similar voids ratio e throughout, η is approximately constant. Using the relationship $\theta = Sr \times \eta$, the van Genuchten's relationship can be rewritten as:

$$Sr = Sr_r + (Sr_s - Sr_r)[1 + (\alpha\psi)^n]^{-m} \tag{2.11}$$

where Sr_r is the residual saturation ratio; Sr_s is the saturated saturation ratio.

A commonly used table for the values of the soil hydraulic parameters in the van Genuchten's SWCC model equation is given by Meyer et al. 1997 using probability distributions. Appendix A contains the Table.

2.3.1 Hysteresis

One characteristic of soil is that when plotting the water retention curves, i.e. saturation ratio versus pore water pressure, it can be observed that the drying curve and the wetting curve follow different paths. This phenomenon is known as hysteresis.

On the drying curve, pore water evaporates from the largest pores first as the capillary action is minimum in largest pores. Pore water then continues to evaporate from increasing small pores until it reaches residual water content. Similarly, on the wetting curve, pore water fills the smallest pores first and subsequently the increasingly large pores. Thus, the two curves follow different paths, causing hysteresis. Due to the hysteresis behaviour of soil, this means that the same soil exposed to the same matric suction can have different saturation ratios depending on whether it is drying or wetting, and on which stage of drying and wetting it is at, as illustrated by Figure 8.

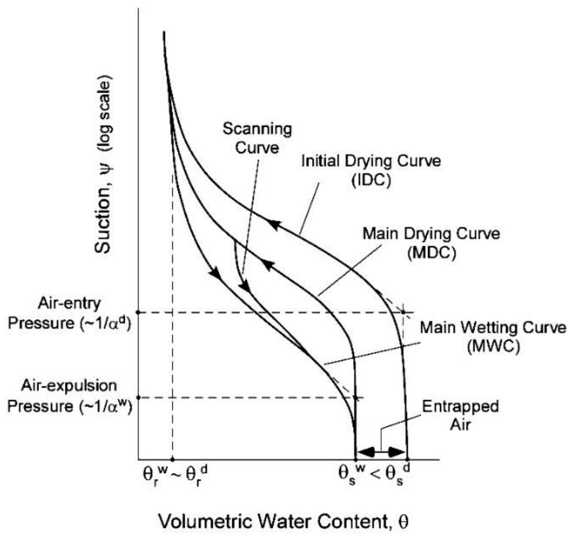

Figure 8. Hysteresis in soils giving different S_r at the same matric suction (Likos et al., 2014)

In order to account for hysteresis, three common constraints can be adopted to scale the main wetting curve from the main drying curve (Kool and Parker, 1987; Nielsen and Luckner, 1992; Simunek et al., 2006):

$$\theta_s^w = \theta_s^d$$

$$\alpha^w = 2\alpha^d$$

$$n^w = n^d$$

However, due to the timescale constraint of this project, hysteresis was not analysed in the numerical analysis presented later in this report.

3. Thermal Expansion of Pipes

In this section, the effects of thermal expansion of pipes on the deterioration of pipes are analysed and discussed.

The axial force due to thermal expansion is given by the equation:

$$P = AE\alpha\Delta\mathrm{T} \tag{3.1}$$

3.1 Possible Modes of Failure

Although there are various possible modes of failure of pipes, only the two most common modes of failure of pipes suggested by previous literature are considered in this report (The Water Services Association of Australia, 2003): joint leakage and upheaval buckling. The axial force (3.1) governs both modes of failure.

3.1.1 Joint Leakage

Joint leakage can be caused by repeated cycles of longitudinal expansion and contraction due to thermal cycles (diurnal, seasonal, annual, etc.). In a healthy pipe network, individual pipes can "slip" slightly within flexible joints. However, in aging pipes where the joints become "locked" or at new joints installed with sub-optimal workmanship, the joints lose the flexibility and stress cycles cause the wear of the joints and hence the joint failure and subsequently leakage.

In this report, the main pipe material considered is polyethylene. In a water main, usually medium or high-density polyethylene (HDPE) pipes are used, which are usually PE80 or PE100 pipes. As specified in BS EN 12201-2 2011, the required hydrostatic strength for PE80 and PE100 pipes at 20°C is 10MPa and 12MPa respectively. Assuming that the welded joints have a similar strength to the minimum required strength of the pipe, the thermal expansion force can be calculated and compared to the minimum required strength to evaluate the likelihood of the joints failing and causing leakage.

For polyethylene pipes, the pipe sections are usually joined together via butt fusion joints. In the case where the joints fail in tension when the two neighbouring pipe sections contract, the thermal force has to overcome both the frictional force between the soil and the pipe and the tensile strength of the fusion joint.

In the analysis, the frictional force along the length of the pipe is considered alongside the strength of the joint. Assuming the joint eventually has negligible strength after ageing, the pipe then relies on the frictional resistance provided by the soil-pipe interface along the length of the pipe to hold the pipe in place. Thus, the frictional resistance was also computed in the sensitivity analysis.

3.1.2 Upheaval Buckling (Blow Out)

Alternatively, pipe sections can also undergo upheaval buckling. The phenomenon is the most common for off-shore pipes where the pipe section lengths are significant compared to the pipe diameter and the thermal variation is extreme. However, upheaval buckling can also occur onshore for shallowly buried pipes where the soil cover is insufficient to resist the upwards buckling force.

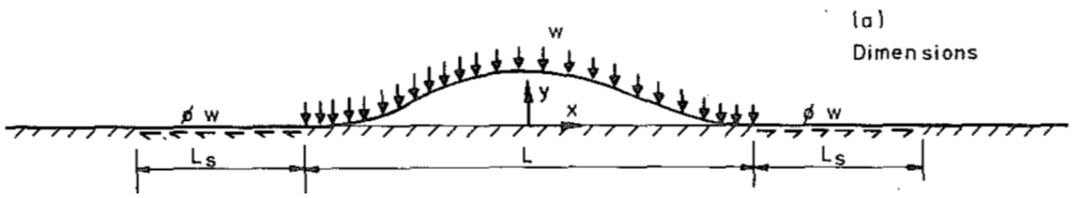

Figure 9. Hobbs vertical buckling mode (elevation view) (Hobbs, 1984)

Various literature in the past has analysed vertical mode buckling using differential equations. In 1972, Kerr published a report reviewing literatures on the vertical instability of railroad tracks, which was then commonly quoted as a basis for developing the vertical buckling mode for pipes and formed the basis for upheaval buckling equations derived after that. In 1984, Hobbs reviewed Kerr's railway track model and published the solutions when having the pipes modelled as railway tracks. In summary, when considering the pipe as a beam column under uniform lateral load equal to the self-weight, by comparing the axial load P in the buckle with the axial load P_0 well away from the buckle, the differential equation describing the buckling mode can be shown to be:

$$P_0 = P + \frac{wL}{EI}[1.597 \times 10^{-5} EA\Phi wL^5 - 0.25(\Phi EI)^2]^{I/2} \quad (3.2)$$

in which Φ is the coefficient of friction between the pipe and the subgrade and w is the weight on the pipe per unit length. (Hobbs, 1984) The equation can then be solved to give:

$$P_0 = 80.76\frac{EI}{L^2} + 1.597 \times 10^{-5}\frac{w^2AEL^6}{(EI)^2} \tag{3.3}$$

where the minimum value of P_0 occurs at the value of L being the buckle length $\bar{L}$:

$$\bar{L} = \left[\frac{1.6856 \times 10^6(EI)^3}{w^2AE}\right]^{0.125} \tag{3.4}$$

By setting the value of w to correspond with different burial depths, the vertical buckling mode can be used to approximate the axial force required for upheaval buckling to occur.

3.2 Evaluation of Frictional Resistance

In evaluating the values of stress, it has been assumed that the analytical solution can be given by considering a pipe as two halves being superposed together.

Figure 10. Breakdown of top and bottom half pipes in the analysis

In case (1), the top half of the pipe experiences stresses primarily due to the soil load vertically above the pipe. In case (2), the bottom half of the pipe experiences stresses primarily due to the soil load vertically above the pipe and the weight of the fluid within.

In both cases, the sum of the normal contact stresses around the pipe periphery governs the available axial resistance, and due to the curved geometry, the sum exceeds the vertical contact force resulting from the pipe weight and the embedment above. Thus, in any resulting calculations, a wedging factor has to be applied to allow for the effects of stress redistribution due to cylindrical geometry.

As given by White and Randolph (2007), the stress expression was derived to be

$$\sigma_n' = \frac{W'\zeta}{D} \tag{3.5}$$

where the wedging factor ζ is given by

$$\zeta = \frac{2\cos\theta}{\theta_{D'} + \sin\theta_{D'}\cos\theta_{D'}} \tag{3.6}$$

and W' represents the effective weight of soil or soil with pipe weight vertically above the section, and $\theta_{D'}$ represents the embedment angle, which in this case is equal to $\pi/2$.

Basic friction equation is given by:

$$\tau = \mu\sigma_n' \tag{3.7}$$

where μ is the soil-pipe interface friction coefficient

By integration, the normal force N, by the soil on the pipe enhanced due to the curved surface can be expressed as:

$$N = W'\frac{2\sin\theta_{D'}}{\theta_{D'} + \sin\theta_{D'}\cos\theta_{D'}} \tag{3.8}$$

Considering the symmetry of the pipe geometry, the wedging factor is assumed to be applicable for the top half of the pipe in a similar manner, with a different definition of θ. Thus, the total frictional resistance along the pipe length is given by

$$F = \mu N \tag{3.9}$$

3.3 Initial Sensitivity Analysis

In order to assess the effects of the variation of different criteria on the stresses experienced by the pipes, an initial sensitivity analysis is carried out by varying each criterion in turn while holding other variables constant, and then checking whether the thermal expansion/ contraction force exceeds the threshold that causes joint leakage or upheaval buckling as described in Section 3.1. The criteria include water table level, burial depth and pipe diameter and thickness.

In the sensitivity analysis, both dry and saturated cases were analysed. However, for simplicity, the extra suction generated by unsaturated soil was not considered in the initial dimensional analysis, and will only be considered in Section 4, where the extra suction strength is generated as a profile using numerical software.

According to the Met Office weather station data, as of 2018, the maximum temperature variation of soil at 1m depth, which is a common burial depth for pipes, is 1.5°C to 21.6°C, i.e. ΔT=20.1°C.

Thus, the thermal force is given by:

$$P = AE\alpha\Delta T = (\frac{\pi D^2}{4} - \frac{\pi(D-2t)^2}{4})E(150 \times 10^{-6})(20.1)$$

The soil is assumed to have a saturated unit weight of 20kN/m^3 and a dry unit weight of 16kN/m^3. Take a value of Φ=30°. The soil-pipe interface μ is assumed to be 0.3.

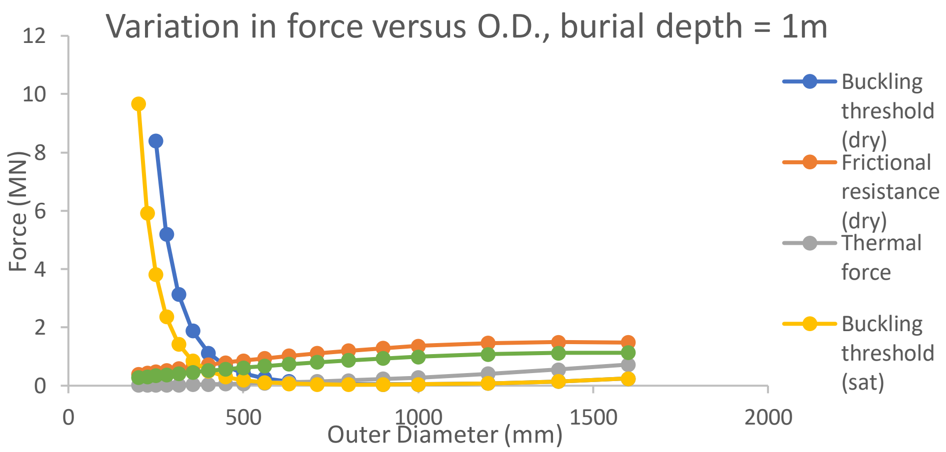

Figure 11. Sensitivity Analysis for varying W.T., burial depth = 1m

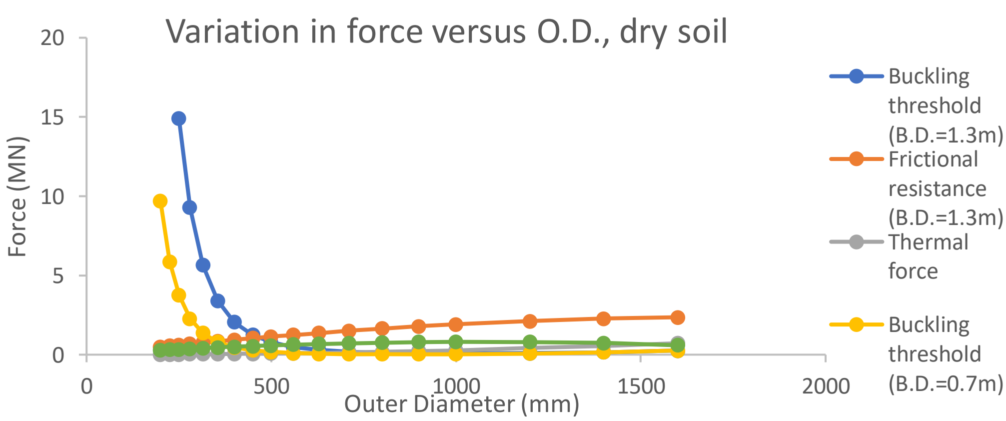

Figure 12. Sensitivity Analysis for varying burial depth, W.T.=below pipe

In Figure 11, the cases where the soil is dry and the soil is saturated were compared. Due to the reduced effective vertical stresses on the pipe, it is not surprising to see that the frictional resistance becomes lower than in the dry case, although the frictional resistance appears to be sufficient to resist axial movement against the thermal loading. However, in both cases where the soil is dry and the soil is saturated, the thermal loading appears to exceed the buckling threshold. Nonetheless, it is uncommon for large diameter pipes to be buried with a burial depth smaller than its diameter (1m), although the specification only requires a burial depth of 0.7m to 1.3m.

In Figure 12, the cases where the burial depth are at the legal lower bound (0.7m) and at the legal upper bound (1.3m) were compared. For the case where the burial depth is only 0.7m, the frictional resistance provided axially becomes lower than the thermal force at large diameter values (i.e. D>1500mm). However again, the purpose of the sensitivity analysis is just to compare the order of magnitude of the forces, and in reality, it is unlikely that a large diameter pipe will be buried with a burial depth smaller than its diameter partial burial. The buckling threshold also exceeds the thermal force for both cases of burial depth.

Although the sensitivity analysis appears to suggest that the pipeline will fail in buckling, it is important to bear in mind that extreme values of temperature range were used. The temperature variation takes place over a yearly cycle, and the soil-pipe interface is likely to be able to dissipate the stresses built-up due to thermal expansion and contraction over time. However, a numerical analysis with more detailed account of different factors is still preferred. Hence, in Section 4, a long-term analysis of the breakout resistance of the soil will be evaluated using Finite Element analysis.

3.4 Uncertainties in Wedging Factor

In the analytical solution of summation of stresses to give the force required to mobilise the soil above the pipe, the “wedging factor” ζ (equation (3.6)) was applied to account for the variation of stresses around the geometry of the pipe. However, such wedging factor was derived by White and Randolph in 2007, purely based on the assumption that the normal stress on the pipe wall varies with $\cos\theta$, where θ is the inclination from the vertical, following the elastic solution for a line load acting on a half-space (White and Randolph, 2007). However, the wedging factor remains in widespread use without any experimental proof. Although $\cos\theta$ appears to have a similar fit to the variation of stresses around the pipe surface, it can be shown that for functions of different orders of $\cos\theta$ can still give a similar trend in the values of stresses while giving very different values at maximum value of stress.

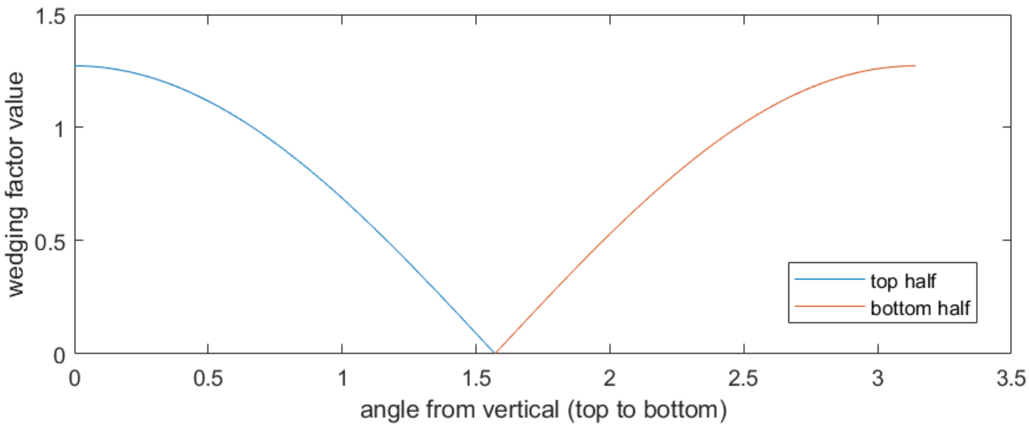

Figure 13. Variation of wedging factor against θ

The wedging factor in use implies that the stress measured at the crown and invert of the pipe would be 1.27 times of the value of the stress measured with the same load acting on a flat surface; similarly, it also implies that the stress measured at the haunch (side) of the pipe would be 0 due to the curved surface and effectively having no weight normally acting on the sides.

Integration then gives

$$N = W' \frac{2\sin\theta_{D'}}{\theta_{D'} + \sin\theta_{D'}\cos\theta_{D'}} \tag{3.10}$$

which gives the value of $N = 1.27W'$ for $\theta_{D'} = \pi/2$

However, different expressions of wedging factor can give similar boundary values for stresses yet give very different values when integrated to give the normal force. For example, a $\cos^2\theta$ function giving the same boundary conditions of ζ could be:

$$\zeta = \frac{2\cos^2\theta}{\theta_{D'} + \sin\theta_{D'}\cos\theta_{D'}} \tag{3.11}$$

Yet when integrated over the surface of the pipe, the normal force would now become

$$N = W' \frac{0.5 \sin \theta_{D'} + \theta_{D'}}{\theta_{D'} + \sin \theta_{D'} \cos \theta_{D'}} \tag{3.12}$$

which now gives the value of $N = 1.32W'$ for $\theta_{D'} = \pi/2$

Thus, a simple experiment was designed in order to verify the accuracy of the wedging factor ζ in currently widespread use in pipeline design.

3.5 Experiment for Wedging Factor Verification

In order to verify the validity of the wedging factor currently in use, a simple experiment was designed to compare the experimental results to the analytical solution of stresses using the wedging factor. Tekscan I-scan sensor pad was used to measure the stresses.

3.5.1 Tekscan system and Calibration for Sensor Pads

The I-scan pad consists of rows of sensors overlapped with columns of the identical sensors. Each overlapping point then sends the measured stress to the Tekscan computer interface.

Figure 14(a). The rows and columns of sensor material on two separate Tekscan I-scan pads.

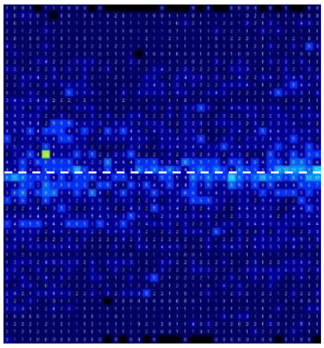

Figure 14(b). Line drawn over a Tekscan stress plot to denote the mirroring of stresses.

The I-scan sensor requires calibration prior to measurements to ensure correct measurement of stresses relative to the soil type. In general, the finer the soil is, the more accurate is the stress measured. To facilitate easier experimental set-up and clean-up, soils that do not leave a residue was preferred to be the soil used in the experiment. Hence, the finest sand (Fraction E sand) available in the Schofield Centre was selected and used to fill the tank (D_{50}=0.18mm). With the sensor laid flat, the calibration was then carried out.

As both faces of sensors on the sensor pad take readings simultaneously, two values of stress readings are essentially obtained for the same point. This means the stress plot is theoretically a mirror image of the stress values of the same points, as shown in Fig 3(b).

For the purposes of this project, the I-scan sensor was roughly calibrated to ensure the interface contact between granular sand and the sensor surface can be accounted for and taken out of consideration in the actual experiment. As discrete points on the pads measure the stress values, the stress spike that granular contact with sand can cause will only show up as a spike on the readings, without any immediately adjacent data to prove that the spike is only caused by the granular contact between sand particles.

In the calibration process, the sensor is laid flat on top of a layer of sand, and covered with more sand on top of the sensor. The weight of sand above and below the sensor was measured and recorded. The sand was compacted each time extra sand was added to the container, to try ensure a similar voids ratio across the sand stratum, so that the sand weight directly above the sensor could be assumed to be proportional to the depth of the sand. After the first measurement was taken for calibration with purely sand on top of the sensor, weights were applied on top of the sand immediately above the sensor in order to achieve a more comprehensive set of calibration data. As the sensor was only shallowly buried, it was assumed that the weight of the weights applied was only taken by the sand immediately above the sensor. The value of weights applied and the corresponding stress values are as shown below:

Calibration Point	Extra weight applied directly above sensor	Total weight applied directly above sensor
0	0 (no sand above sensor)	0
1	8.89N sand	8.9N
2	5.23N sand	14.12N
3	19.62N weight (2kg)	33.6N
4	14.72N weight (1.5kg)	48.3N

Table 1. Weights used for the calibration of Tekscan I-scan sensor pads

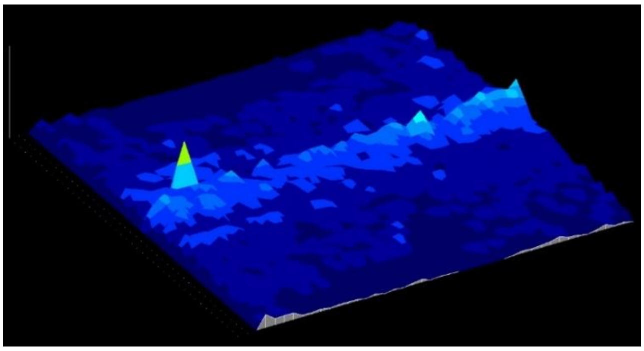

Figure 15(a). Stress visualisation interface showing stress spikes

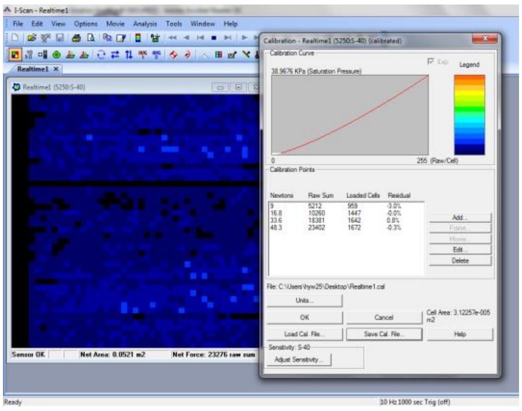

Figure 15(b). Calibration process on the user interface

3.5.2 <u>Design of Setup</u>

In the experiment, a cylinder with a diameter of 65mm was cut to the length of exactly 180mm such that it could fit into a tank with dimensions being 720mm×180mm. The mass of the cut cylinder is 1.57kg. The I-scan sensor pads used were 110mm×110mm by area. The shallow burial depth was an experimental limitation, which will be discussed later.

Figure 16(a). Overall setup showing the container tank and the Tekscan handle connected to the sensor during the calibration process.

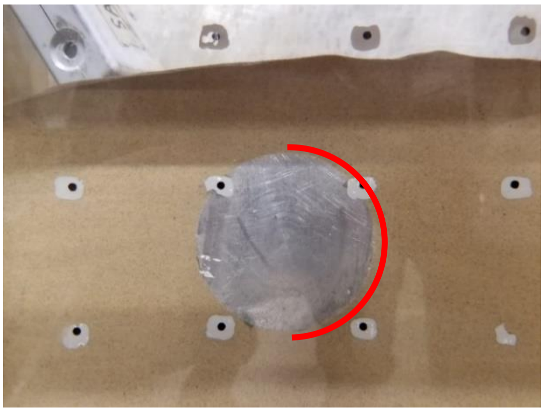

Figure 16(b). A close-up shot of the shallowly buried cylinder, with the red line denoting the position of the I-scan pad wrapped around the cylinder.

After calibration, the I-scan sensor pad was first wrapped around the cylinder before being buried into the sand to give a set of readings purely due to the wrapping effect. The stress values were recorded and the cylinder was then buried into the sand. This is to account for the offset due to wrapping the originally flat sensor around the cylinder. In doing this, it was assumed that the stresses caused by the wrapping are normal to the sensors, hence making the stresses caused by wrapping and the stresses caused by loading directly superposable.

The burial depth was approximately 3.2cm, which was about half of the diameter of the cylinder. The main reason for the shallow burial depth is due to the technical constraint of having to protect the Tekscan handle from sand, as any entry of sand into the Tekscan handle could potentially cause the malfunctioning of the handle in outputting values to the computer interface.

3.5.3 Experiment Results

The obtained stress values were averaged between the same data points read by the two faces of the sensor. Moreover, as the cylinder was subjected to the same load throughout the length (plane strain conditions), the stress reading was also averaged over the length of the cylinder to give only one value of stress for each value of angle from the vertical.

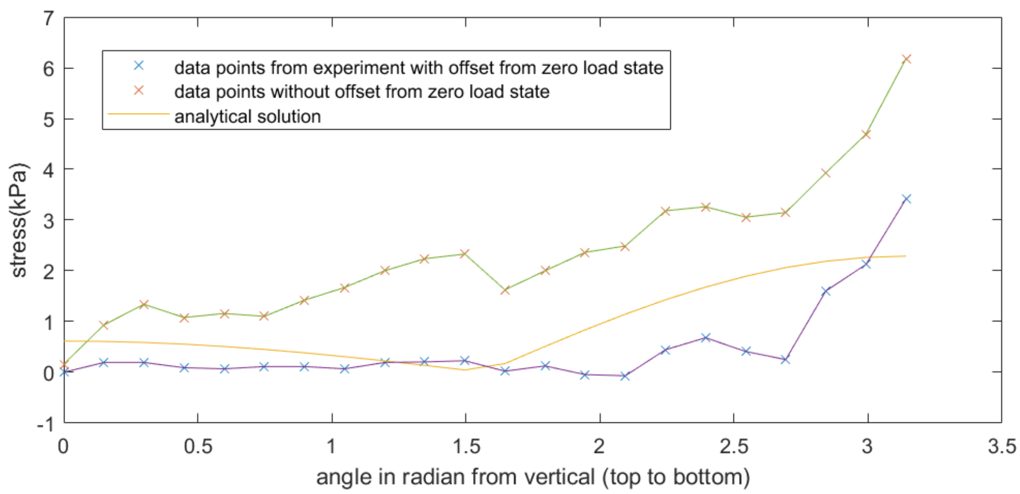

Figure 17. Experimental results plotted alongside analytical solution

The experimental results with, and without offset from zero load state were plotted alongside the analytical solution obtained using the wedging factor as given by White and Randolph (2007). As seen in Figure 17, the two lines representing the experimental values give the allowable region of where the analytical solution lies. The offset due to zero offset state was actually very large compared to the readings after the offset from zero load state. Thus, the allowable region remains relatively large and did not provide a precise trend for the comparison with the analytical solution. However, the analytical solution in general roughly lies within the allowable region, although the trend could not be compared directly.

At the haunch of the cylinder, the analytical solution denotes that the measured normal stresses acting on the cylinder should be zero. However, the experimental readings after offset fell below 0 at this point, which indicates that the assumption of the stresses due to the wrapping around the cylinder and the stresses due to the load being directly superposable is quite likely incorrect. Moreover, as the offset is the larger at this point relative to the low normal stresses that would normally be present at the haunch of the cylinder, it is difficult to deduce the actual value of normal stresses that should have been measured.

Moreover, at the invert of the cylinder, the analytical trend seemed to have deviated considerably from the experimental values. It was intended that the experiment should be repeated to further verify the wedging factor, most likely with the use of hydraulic press such that the offset due to zero load state can become negligible. However, due to the COVID-19 pandemic, further experiments were not possible in Lent term.

Thus, verifying the wedging factor experimentally is considered to be an item for future work. The simplicity of the setup means that it should not take much effort to complete the verification.

4. Effects of Suction due to Unsaturated Soil

As explained in Section 2 and Section 3, this Section focuses on exploring the extra strength available to the soil matrix due to the unsaturated properties of the soil.

$$\tau_f = c' + (\sigma - S_r u_w - (1 - S_r)u_a)tan\,\varphi' \quad (4.1)$$

For the case of shallowly buried pipelines, pore air is approximately atmospheric, hence giving $u_a = 0$. The expression for shear strength of soil above the ground water level then reduces to:

$$\tau_f = c' + (\sigma - S_r u_w)tan\,\varphi' \quad (4.2)$$

Without considering the suctional strength due to capillary action, i.e. not considering the effects of negative pore water pressure, the shear strength above the ground water level would be given by:

$$\tau_f = c' + \sigma' tan\,\varphi' = c' + \sigma tan\,\varphi' \quad (4.3)$$

Subtracting the two equations gives an expression for the extra shear strength component due to matric suction of:

$$c'_{suction} = -S_r u_w tan\,\varphi' \quad (4.4)$$

$c'_{suction}$ can be considered as the cohesion available to the soil matrix due to the capillary action under negative pore water pressure.

4.1 Analysis Using Optum CE

Optum CE is a Finite Element analysis software that can be used to analyse different geotechnical problems, from shallow foundation analysis to seepage and groundwater flow. There are various failure criterions available for use as materials in Optum CE, including Tresca failure criterion and Mohr-Coulomb failure criterion. Mohr-Coulomb criterion was used in this analysis.

By using an MC soil, the user interface allows the user to input c' and φ', either as a constant or a profile to be imported. Using Equation (4.4), the cohesion available within the soil matrix due to suction was input into the strength criterion as c to investigate the impact of the extra available strength due to matric suction alone. The $c'_{suction}$ profile was generated via Matlab by determining the values of S_r using the van Genuchten's SWCC modelequations.

Similar to the sensitivity analysis conducted in Section 3, there are various criteria of interest and these variables are varied in turns in order to investigate the effect of these variables on the extra shear strength available within the soil. These variables are:

(1) Soil Types
(2) Water Table
(3) Friction Angle (while holding other soil properties constant)

In each case, the results from running a lower bound analysis were then used to plot a V-H envelope to determine the effect of these parameters on the shear strength of the soil. The V-H envelopes were then compared to existing V-H failure envelopes from the literature. In this project, the drained failure envelope derived by Tom and White et al. (2019) were used for comparison.

4.2 <u>Design of Model</u>

The model consists of a pipe of 2m diameter where its wall thickness is assumed to be negligible. The burial depth is 1m and the soil is normally consolidated. The soil stratum is designed to be 10m deep and with a large width compared to the depth such that plane strain conditions can be assumed. By "probing" the pipe with different load angles, the load can be resolved into V and H to give a V-H combination at failure. The load cases are at an increment of the load angle of 10° and spans from 0° to 180°. Non-associated flow conditions were used. As long-term failure is the topic of interest, drained analysis was carried out. In any case, modelling c' suction as c' implicitly includes the effects of pore suction/ pressure.

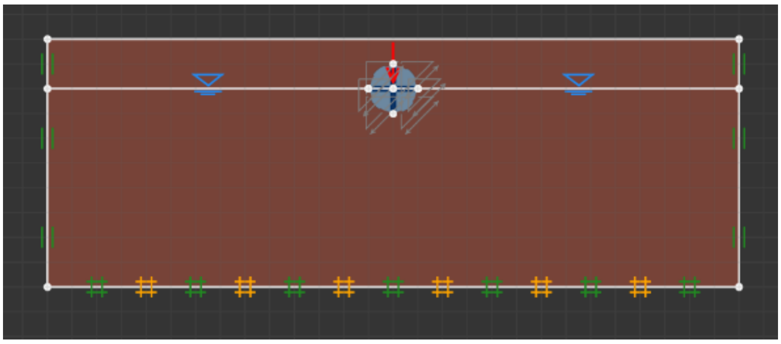

Figure 18. Screenshot within Optum CE showing the layout of the model

For the soil-pipe interface, the interface joint material was assumed to have the same properties as the soil. This assumes that the interface behaves as a rough/no tension shear joint, which gives the most realistic failure envelope. Two rigid plates were added across the centre of the pipe cross-section perpendicularly to represent the constraint against the "probing" load rotating within the pipe.

4.3 Profiles of c'

Firstly, the case of different soil types was considered. The soil types considered are clay, silty clay and sand. The soils were assumed to have the same friction angles and the same unit weight for simplicity. The only difference in the soil properties used in the model were the soil hydraulic properties and the values of parameter from the Table in Appendix A. Using the parameters as given in Appendix A, the c' profile can be generated as shown in Figure 19(a).

Three values of ground water level were also considered. The W.T. values of 1m and 2m represent the cases of the W.T. at the crown of the pipe and the middle of the pipe respectively. The W.T. value of 10m represents the case when the water table is sufficiently far from the pipe. The corresponding c' profiles are as shown in Figure 19(b).

The same soil with two different values of friction angles φ' was also analysed, with the values of φ' being 30° and 35° respectively, which is shown in Figure 19(c).

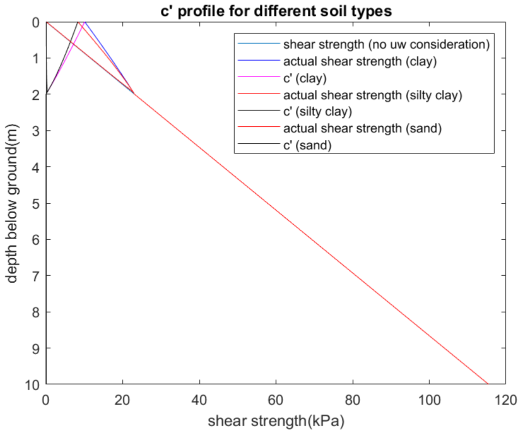

Figure 19(a). c' profile for different soil types, W.T.=2m

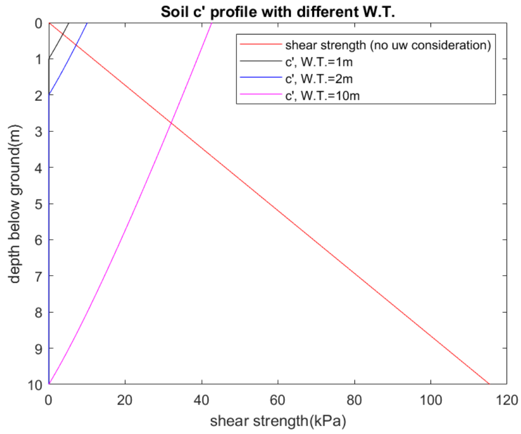

Figure 19(b). c' profile for different water tables

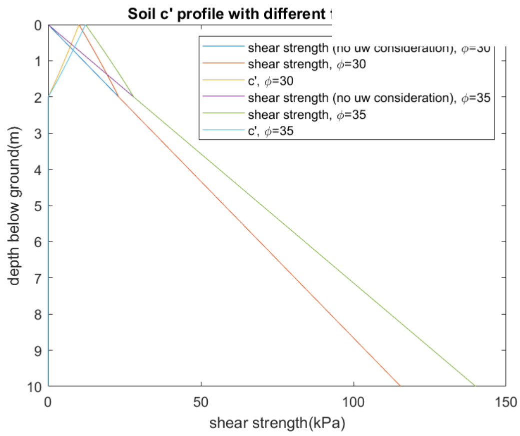

Figure 19(c). c' profile for different φ' values

In terms of the c' profiles, it should be noted that the S_r indicates an ever increasing suctional strength due to negative pore water pressures, i.e. increasingly deep water table. Using the theory of capillary rise, it can be shown that there is a specific height above which capillary suction does not occur as the surface tension is not large enough to support the suction, hence above the maximum capillary height the soil is free from the influence of ground water and this region of soil is either dry or saturated depending on surface waters. However, the c' profile was still used for the analysis for assessing the difference at extreme values of capillary suction.

4.4 V-H Failure Envelopes from Analysis

The c' profiles were imported into Optum CE with the methodology described in Section 4.2 to obtain values for V and H. The V-H envelopes were analysed in two different ways:

(1) In Section 4.4.2, V and H were normalised with the V_{max} in each respective case alongside V-H failure envelope proposed by previous literature. The V-H failure envelope chosen from literature has the characteristic where the V-H failure envelope is independent of the three factors of interest as mentioned in Section 4.1. This is to testify whether the failure relationship can be written in terms of parameters that are independent of the factors of interest.
(2) In Section 4.4.3, V and H were normalised with the largest V_{max} values across all cases. This is to compare the change in values and shapes of the envelope due to changes in the same variable.

4.4.1 Drained Failure Envelope – Tom and White (2019)

Due to the lack of failure envelopes for shallowly buried pipelines in previous literature, failure envelopes for partially embedded were used with caution for comparison instead. Two commonly used V-H failure envelopes for pipe breakouts were plotted alongside the results obtained using Optum CE analysis with the c' profiles obtained above. These envelopes were derived with the finite element models with partially embedded pipes.

A drained failure envelope was derived by Tom and White (2019) using Finite Element analysis. The failure envelope was derived with the values of w/D ranging from 0.1 to 1, assuming weightless soil. This makes the model quite likely to be a suitable candidate to generate a failure envelope for a buried pipeline. The failure envelope is given by:

$$\frac{\bar{H}}{\bar{V}_{max}} = \mu\left(\frac{\bar{V}}{\bar{V}_{max}} + \beta\right)^{n}\left(1 - \frac{\bar{V}}{\bar{V}_{max}}\right)^{m} \tag{4.5}$$

where $\bar{H}$, $\bar{V}_{max}$ and $\bar{V}$ are dimensionless quantities given by:

$$\bar{V} = \frac{V}{\gamma' D^2}\ ;\ \bar{V}_{max} = \frac{V_{max}}{\gamma' D^2}\ ;\ \bar{H} = \frac{H}{\gamma' D^2}$$

and the parameters μ, n and m are given by:

$$\mu = \frac{0.2w}{D} + \mu_0\ ;\ \mu_0 = -0.00437\varphi_{peak} + 0.42; m = 0.013\varphi_{peak} + 0.4\ ; n = 0.64$$

β represents the maximum vertical uplift (tension) capacity as a proportion of the maximum (downward) vertical capacity, which can be taken as $|\bar{V}_{min}/\bar{V}_{max}|$.

In the analysis, when plotting the failure envelope as suggested by Tom and White (2019) alongside V-H envelope as obtained from Optum, the value of w/D is taken to be 3/2=1.5.

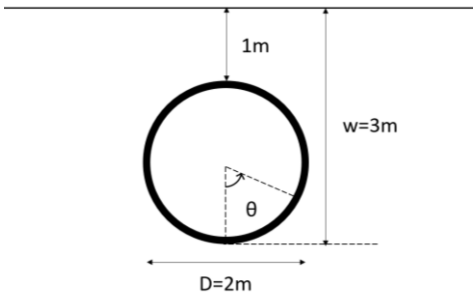

Figure 20. Problem definition showing $w/D = 1.5$

4.4.2 V-H Envelopes Comparison with Literature

The V-H failure envelopes using Tom and White (2019)'s model were plotted with the value of φ_{peak} being 30° for the plots for different soil types and different ground water level; and φ_{peak} being 30° and 35° for the plot for different soil friction angles.

Regarding the value of β, both $\beta = 0$ and $\beta = |\bar{V}_{min}/\bar{V}_{max}|$ were plotted separately for clarity and the plots were then compared.

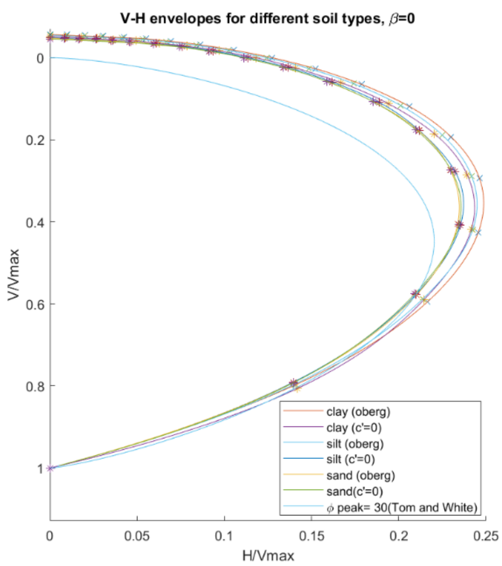

Figure 21(a). V-H envelopes for different soil types, $\beta = 0$

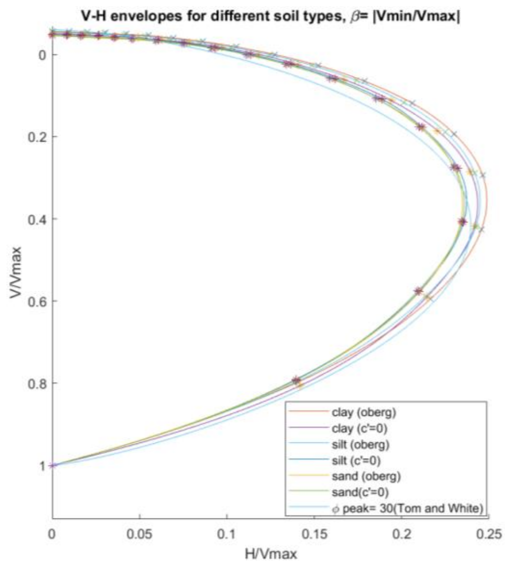

Figure 21(b). V-H envelopes for different soil types, $\beta = |\bar{V}_{min}/\bar{V}_{max}|$

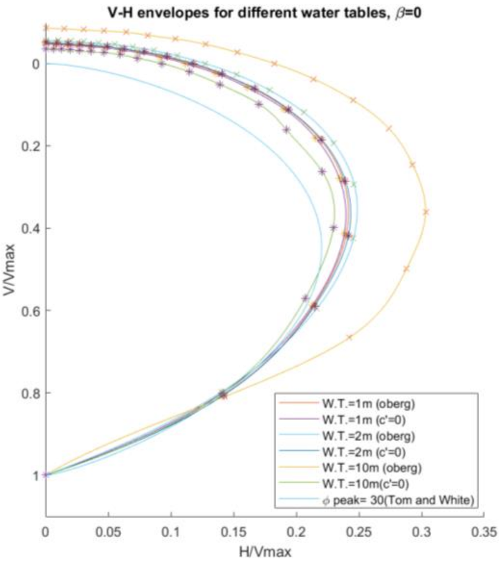

Figure 22(a). V-H envelopes for different water tables, $\beta = 0$

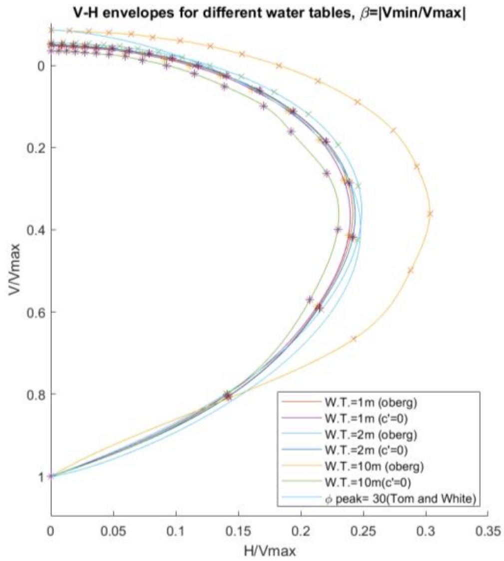

Figure 22(b). V-H envelopes for different water tables, $\beta = |\bar{V}_{min}/\bar{V}_{max}|$

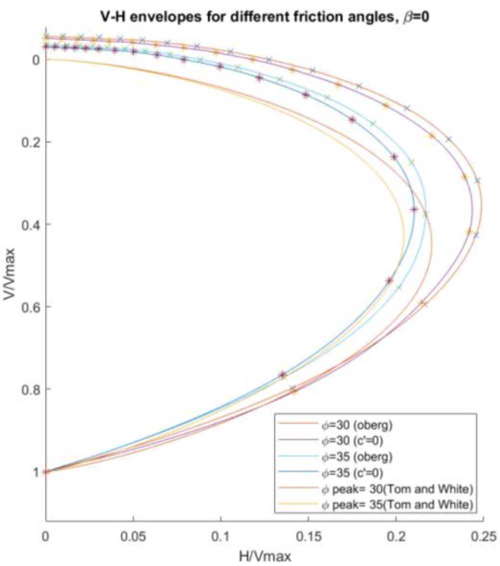

Figure 23(a). V-H envelopes for different friction angles, $\beta = 0$

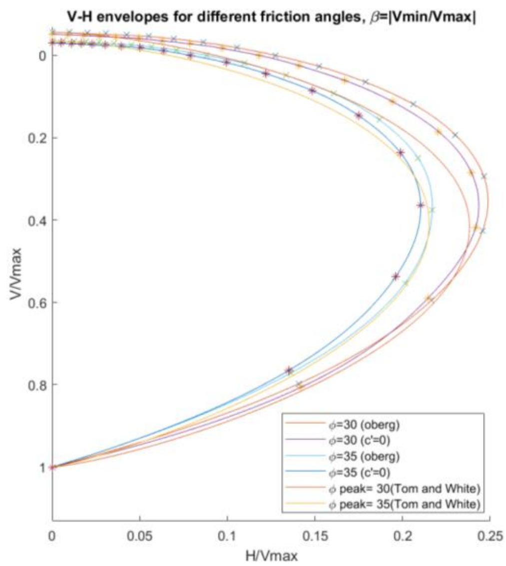

Figure 23(b). V-H envelopes for different friction angles, $\beta = |\bar{V}_{min}/\bar{V}_{max}|$

In the above plots, negative values of V represent an upward acting V. By setting $\beta = |\bar{V}_{min}/\bar{V}_{max}|$, Tom and White's model can have the same boundary values as the failure envelope derived from Optum CE. Surprisingly, Tom and White's model actually appeared to be a good approximation of the V-H envelope in most cases. The main deviation is that the failure envelope calculated using results from Optum CE appears to be more skewed toward the negative V/V_{max} axis than the failure envelope derived using Tom and White's model.

Another discrepancy is that the model seems to consistently underestimate the value of H/V_{max} at low values of V/V_{max}. At negative or low values of V/V_{max}, the “probing” load acts upwards or close to the horizontal, it is mainly the soil above the pipe that helps resist the breakout. This suggests that the unsaturated properties of the soil are likely to have enhanced the shear strength of the soil and enabled the soil to have a higher shear strength than that predicted by Tom and White’s model. However, the values of the V-H relationship in general appear to be relatively close.

The V-H envelope for the water table at 10m below ground proved that the expression for S_r should be used with extreme care. As the expression does not involve checking the maximum capillary height of the soil, the expression could mislead the users to think that the extra shear strength resulting from capillary suction could keep increasing. However, upon a rough calculation, it can be shown that the soil analysed does not have the maximum capillary height of 10m, hence giving the large discrepancy in the V-H envelopes.

Tom and White’s model when $\beta = 0$ appears to largely underestimate the values of H/V_{max} regardless of the values of V/V_{max}, which proves that the model would have been overly conservative if it was used for design.

It was attempted to suggest an expression for the V-H envelopes derived from Optum analysis with the curve fitting tool in Matlab. It was found that after being normalised by the V_{max} in each respective case, the V-H envelopes can be roughly fitted on a rational with a quadric numerator and a quadratic denominator. However, due to time constraints, repeated runs were impossible and coefficients for the function of best fit could not be found. As large discrepancies between V-H envelopes were only observed in the plot for different soil friction angles, it can be proposed that H/V_{max} is definitely a function of V/V_{max} and the soil friction angle. While the influence on the shape of V-H envelope due to soil type and its respective hydraulic parameters do not seem significant, no clear conclusion can be drawn about the influence on the V-H envelope due to changes in water table.

Another observation is that it is quite likely that the extra lateral breakout capacity due to capillary suction is non-linear. This can be observed in the uneven differences between V-H envelopes considering and without considering negative pore water pressure effects for each case. Thus, it is possible that the V-H failure envelope could be an expression involving influences due to pore water pressure changes, if there really exists a V-H failure envelope that can describe the behaviours of a shallowly buried pipes in unsaturated soils.

4.4.3 V-H Envelopes Comparison by Factor

In this Section, the values of H are divided by a consistent V_{max}, that is, the largest V_{max} among the cases for the factor concerned.

For the case of different soil types, the V and H values are all divided by the V_{max} found in the case of clay where u_w is considered, as plotted in Figure 24(a).

For the case of different water tables, the V and H values are all divided by the V_{max} found in the case of W.T.=10m where u_w is considered, as plotted in Figure 24(b).

For the case of different friction angles, the V and H values are all divided by the V_{max} found in the case of φ =35° where u_w is considered, as plotted in Figure 24(c).

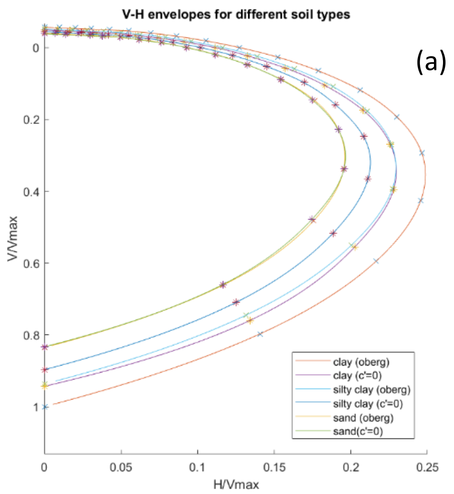

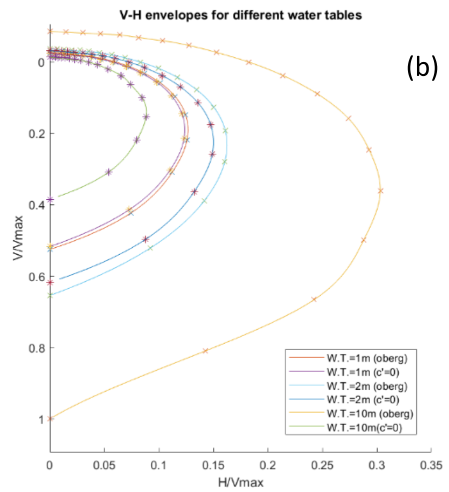

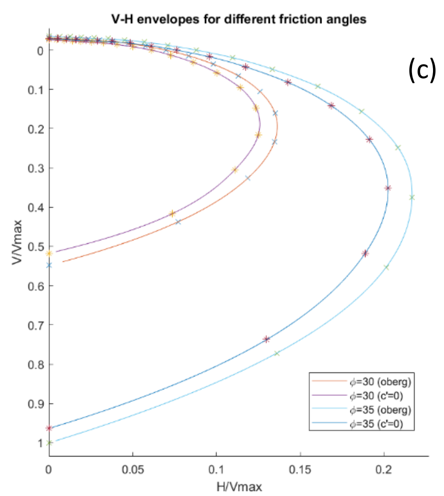

Figure 24(a). V-H envelopes for different soil types

Figure 24(b). V-H envelopes for different water tables

Figure 24(c). V-H envelopes for different friction angles

In Figure 24(a), the effects of soil types on the V-H failure surface were explored. As expected, the extra lateral breakout capacity due to negative pore water pressure was the largest in clay, then followed by silty clay and then sand. As observed in the c' profiles (Figure (19)) the c' profile for sand due to capillary suction was very close to zero, due to the adjustment in soil water-retention characteristics with the use of the parameters in the Table in Appendix A. However, although the extra c' available due to unsaturated soil behaviour was much greater in clay than that available in sand, when comparing the ratios of H/V_{max}, the lateral breakout resistance in clay was actually just about 1.24 times of that of sand, which reflects that the water-retention characteristics of the soil might have a lesser effect on the V-H envelope than water table and friction angle of the soil.

In Figure 24(b), the effects of varying water table on the V-H failure surface were explored. As mentioned above, it is quite unlikely the soil will be unsaturated throughout the 10m depth. Nonetheless, it can be clearly observed that increasing the depth of water table increases the value of $c'_{suction}$ rapidly. The implication is that fluctuation in ground water level can greatly affect the available breakout resistance, and this should be taken into account when designing for buried pipes in regions where the soil is likely to be unsaturated.

In Figure 24(c), it can be observed that the available lateral breakout resistance increases drastically with a 5° increase in the value of φ. The implication is that again fluctuation in the soil friction angle can greatly affect the available lateral breakout resistance. For example, if the installation techniques for the pipes are poor and the surrounding soil was disturbed, this can potentially loosen an initially dense soil stratum and decrease the lateral breakout resistance.

4.5 Implications on Backfill Material in Construction

In reality, after pipe installation, soil is backfilled into the excavated pit up to the original ground level. In most cases, the original soil that was in place would be sufficient as backfill material, but good compaction would be required to ensure the soil is not too loose, in order to attempt to restore the original value of friction angle. This heavily relies on the workmanship of the contractor, and the consequences of insufficient compaction hence a lower friction angle than original is of interest. Thus, a $c'_{suction}$ profile was generated where the soil above the invert level is of a lower friction angle than the soil in-situ. The $c'_{suction}$ profile was then imported into Optum to obtain a V-H envelope to be compared with the V-H envelope where the soil is of a consistent friction angle throughout. In this analysis, the "incorrect" case consists of φ =35° above the invert level of 3m, and φ =35° below 3m; the "correct" case consists of φ =35° throughout the soil stratum. The water table is set to be at 5m depth such that the unsaturated behaviours of the soil can be observed more clearly.

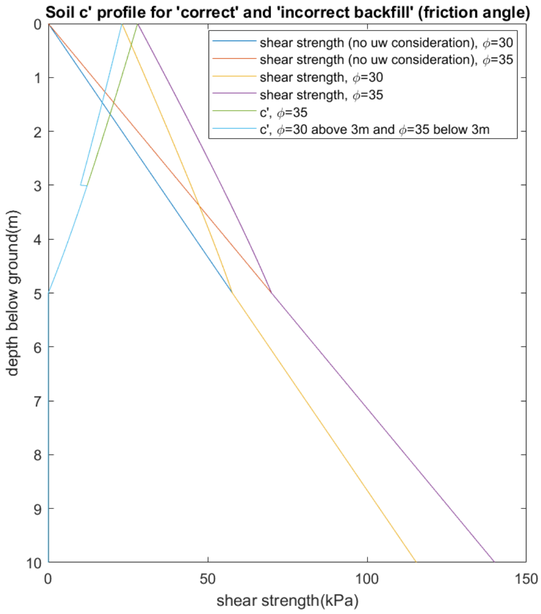

Figure 25(a). c' profile for 'correct' and 'incorrect' backfills w.r.t friction angle

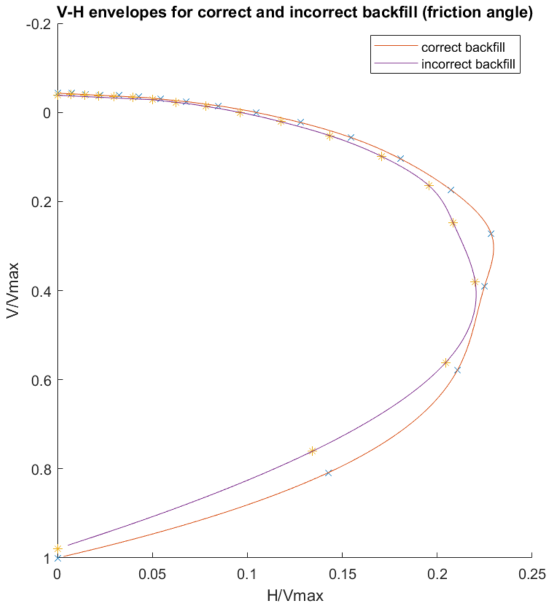

Figure 25(b). V-H envelopes for 'correct' and 'incorrect' backfills w.r.t friction angle

Similar to the case where the water table was set to be at 10m depth in Section 4.4, the van Genuchten's SWCC model equations assumed an ever-increasing shear strength with the increasing height of soil above the water table, which in reality is not the case. However, it can still be observed that there is a considerable gap between the two V-H envelopes when the values of V and H obtained in both cases were divided by the Vmax value obtained in the analysis using the correct backfill with the friction angle of φ =35° throughout. This result implies that good compaction technique should be practised and it might be unconservative to assume that the backfill has the same friction angle as it did before being excavated.

Moreover, another subject of interest is when the contractor uses another material as backfill instead of the soil originally in-situ. Quite often, less cohesive backfills such as sandy backfill is preferred over silty or clayey backfill as compaction would not be required by the specification. Thus, analysis was also carried out to compare the cases where the backfill consists of sand and the backfill consists of silty clay when the soil in-situ is silty clay. The 'correct' case consists of sand above the invert level of 3m and silty clay below 3m; the 'incorrect' case consists of silty clay throughout the soil stratum. The backfill sand is assumed to have the same unit weight as the silty clay in-situ.

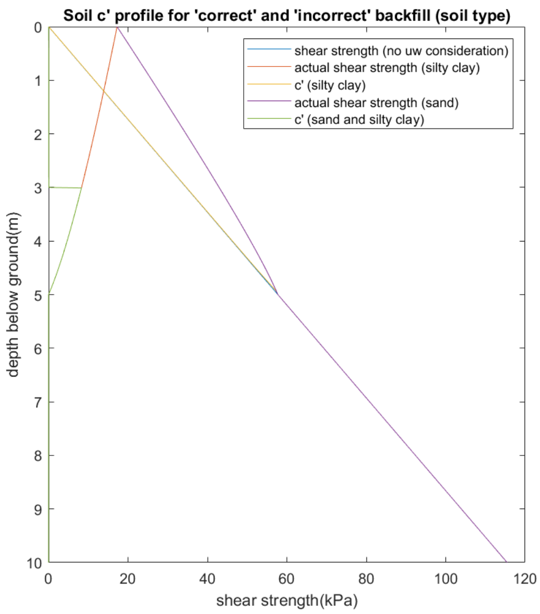

Figure 26(a). c' profile for 'correct' and 'incorrect' backfills w.r.t soil type

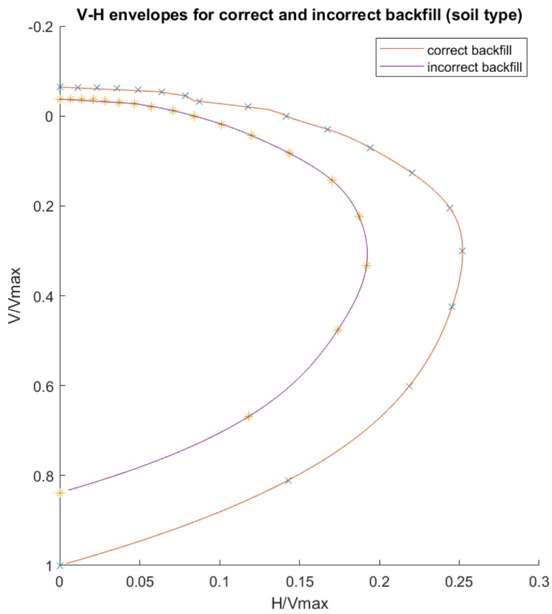

Figure 26(b). V-H envelopes for 'correct' and 'incorrect' backfills w.r.t friction angle

The analysis suggested that choosing a sandy backfill over a silty clay backfill gives a smaller V-H envelope. This suggests that the silty clay fill gives the soil stratum a significantly larger shear strength than using a sandy fill. However, in reality, it is more difficult to ensure a silty clay fill is compacted well compared to a sandy fill, and insufficient compaction could result in unwanted movement of the pipe under different loading, which could exacerbate the shearing in joints. Thus, the designer should evaluate the soil type accordingly and weigh the consequences and costs of using a less cohesive backfill but minimising pipe movement and using a more cohesive backfill but requiring better compaction and hence workmanship.

It should be noted that the limitation of the free Optum academic license is that there could only be 2 materials in a case, which means it was impossible to have more than 1 type of soil in a case. However, as the $c'_{suction}$ profile was derived and then imported into Optum and the analysis was for long-term failure, this means the soil-water retention characteristics of the soil could be imposed onto the model, which is an advantage of using the van Genuchten's SWCC model equations and the Öberg and Sällfors relationship. However, one inaccuracy that should be rectified when more soil types are allowed to be introduced into the model is that, the soil above the invert level does not consist of entirely soil of the backfill type, which was assumed in the analysis carried out in this report. As shown in the failure animation in Optum, some 'probing' angles could mobilise quite a large volume of soil, which in reality would have consisted of less backfill as the excavated pit would not have extended that far away from the pipe, as illustrated in Figure 27.

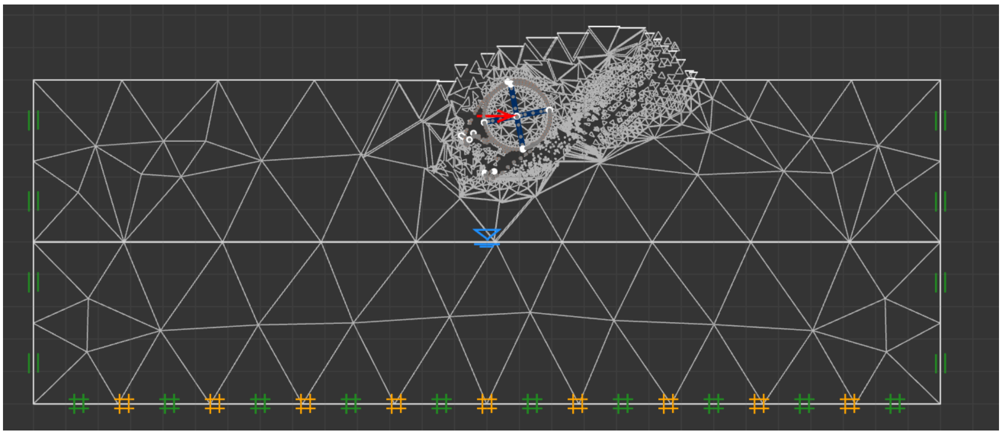

Figure 27. Optum deformation animation showing that a 'probing' angle of 90° mobilises soil far away from the initial pipe location

All in all, the analysis shows that the soil type or friction angle of the backfill can have profound impacts on the soil stratum shear strength, as these factors can vary the soil-water retention characteristics of the soil matrix greatly. Thus, the designer should take extra caution when deciding the suitable backfill for the specific site and make sure the contractor follows the design accordingly.

5. Conclusion

5.1 Main Findings

Going back to the aim of developing fundamental understanding the basic mechanisms of bursts and leakage, the analysis conducted in this Project compared analytical solutions from various previous literature and shed light onto the possible directions for improving numerical analysis in the future.

As highlighted via the sensitivity analysis in Section 2, it has been found that there is a possibility where the thermal force caused by temperature cycles could exceed the vertical buckling threshold. However, a more detailed analysis of temperature variations over the yearly cycle would be required to make further advance in determining whether the soil-pipe interface has sufficient time to dissipate the stress built-up due to temperature differences. It has been concluded that if there is insufficient time for the pipes to dissipate the stress built-up, the pipe could fail under vertical buckling. Although the failure might not be as severe as an upheaval buckling failure, significant leakage could still result due to over-shearing any pipe joints.

The wedging factor used in deriving the stresses around a pipe and hence in the expression of forces acting around the pipe has been used in literature throughout the years without any verification. It has been concluded that although it seems reasonable that the function is some function of $\cos\theta$, the large possible discrepancy that could be caused by a different function of $\cos\theta$ suggests that further experiments should be conducted to verify the actual function for the wedging factor.

Finite Element Analysis was used to analyse the extra shear strength available to a soil matrix due to the capillary suction in unsaturated regions. It was found that, surprisingly, the drained failure envelope proposed by Tom and White (2019) for a partially embedded pipe was a decent fit to the failure envelopes derived using a shallowly buried pipeline by using Optum CE. This suggests that there is a possibility that there could exist a failure envelope with a similar form to the model proposed by Tom and White (2019) that can give the normalised breakout capacity for a soil. A possibility of an expression with a rational of a quadric numerator and a quadratic denominator was also proposed. However, the actual expression was not found in the report due to time constraint.

Moreover, it was found that varying the factors of interest in a shallowly buried pipe model affect the shape and values of the V-H envelopes to very different degrees. By observing the extent of influence of each factor on the V-H envelope, it was concluded that the water-retention characteristics of a soil are most likely unimportant to the long-term V-H failure envelope of a shallowly buried pipeline. Efforts should be focused on finding a form that fits the results derived using finite element analysis such that water companies can better conclude the possible behaviours of their pipes over time and narrow down the range of pipes that possibly need repair.

5.2 Future Work

This project laid the path pointing out the directions with possible further developments in the future to be made such that the basic mechanisms of burst and leakage could be better understood.

Firstly, with increasingly extreme weather, better data or prediction on temperature cycles should be obtained such that analysis on the thermal expansion/contraction cycle of a pipe buried at a nominal depth could be conducted. Numerical modelling can be used such that the pipe properties can be modified to simulate an older pipe instead of freshly installed pipe. This way, the water companies could better pinpoint the pipes that need repair.

Moreover, efforts should be spent to find a relationship between the stresses acting on a pipe and its geometry. The wedging factor experiment designed was low-cost and simple, yet helps to testify something with possible profound implications. The experiment should be repeated in a larger number of runs in the future such that the wedging factor could be verified.

Last but not least, with the parameter analysis done via Optum results, work can be done to investigate the possible form of best fit for the V-H envelopes for a shallowly buried pipeline in unsaturated soil in general. With such equation, the behaviour of a pipe and the extra shear strength available can be understood with a generalised simple analysis, which is useful when there are numerous pipes around the UK that possibly need repairing.

References

Escario, V. and Sáez, J., 1986. The shear strength of partly saturated soils. *Géotechnique*, 36(3), pp.453-456.

Farrow, J., Jesson, D., Mulheron, M., Nensi, T. and Smith, P., 2017. *Achieving Zero Leakage By 2050: The Basic Mechanisms of Bursts and Leakage*. [online] UK Water Industry Research Limited. Available at: <https://ukwir.org/view/$UdHWgsG!> [Accessed 5 May 2020].

Fredlund, D. and Xing, A., 1994. Equations for the soil-water characteristic curve. *Canadian Geotechnical Journal*, 31(4), pp.521-532.

Hobbs, R., 1984. In-Service Buckling of Heated Pipelines. *Journal of Transportation Engineering*, 110(2), pp.175-189.

Khalili, N. and Khabbaz, M., 1998. A unique relationship for χ for the determination of the shear strength of unsaturated soils. *Géotechnique*, 48(5), pp.681-687.

Kool, J. and Parker, J., 1987. Development and evaluation of closed-form expressions for hysteretic soil hydraulic properties. *Water Resources Research*, 23(1), pp.105-114.

Meyer, P. D., Rockhold, M. L., and Gee, G. W., 1997. Uncertainty analyses of infiltration and subsurface flow and transport for SDMP sites. Rep. NUREG/CR-6565, PNNL-11705, U.S. Nuclear Regulatory Commission, Washington, DC.

Nielsen, D. R., and Luckner, L. M., 1992. Theoretical aspects to estimate reasonable initial parameters and range limits in identification procedures for soil hydraulic properties. Proc., Int. *Workshop on Indirect Methods for Estimating the Hydraulic Properties of Unsaturated Soils*, M. Th. van Genuchten, F. J. Leij, and L. J. Lund, eds., Univ. of California, Riverside, CA, 147–160.

The Daily Mail, 2019. Britain's biggest water company loses 152million gallons every day through leaks with 25% its supply to customers never reaching homes and businesses. [online] Available at: <https://www.dailymail.co.uk/news/article-7291511/Britains-biggest-water-company-loses-152million-gallons-day-leaks.html> [Accessed 4 May 2020].

The Standards Policy and Strategy Committee, 2011. *BS EN 12201-2:2011+A1:2013 Plastics Piping Systems for Water Supply, And for Drainage and Sewerage Under Pressure — Polyethylene (PE)*.

The Water Services Association of Australia, 2003. *Common Failure Modes in Pressurised Pipeline Systems*.

Tom, J. and White, D., 2019. Drained Bearing Capacity of Shallowly Embedded Pipelines. *Journal of Geotechnical and Geoenvironmental Engineering*, 145(11).

Peachey, A., 2020. The Leakage Challenge. [online] *Water & Wastewater Treatment Online*. Available at: <https://wwtonline.co.uk/features/the-leakage-challenge> [Accessed 4 May 2020].

Simunek, J., van Genuchten, M. Th., and Sejna, M., 2006. The HYDRUS software package for simulating two- and three-dimensional movement of water, heat, and multiple solutes in variably-saturated media, *PCProgress*, Prague, Czech Republic.

White, D. and Randolph, M., 2007. Seabed Characterisation and Models for Pipeline-soil Interaction*. International Journal of Offshore and Polar Engineering*, 17(3), pp.193-204.

Zhou, A. and Sheng, D., 2009. Yield stress, volume change, and shear strength behaviour of unsaturated soils: validation of the SFG model. *Canadian Geotechnical Journal*, 46(9), pp.1034-1045.

Appendix A – Table of parameters in the van Genuchten's SWCC equation (Meyer et al., 1997)

Table 1. Probability Distributions for Soil Hydraulic Parameters Differentiated by Soil Texture (Adapted from Meyer et al. 1997)

Soil texture (USDA)	α (kPa^{-1}) Distribution type	μ	σ	n Distribution type	μ	σ	θ_s Distribution type	μ	σ	θ_r Distribution type	μ	σ
Sand	N	1.50	0.26	LN	2.67	0.27	N	0.43	0.06	LN	0.05	0.01
Loamy sand	N	1.28	0.41	LN	2.27	0.21	N	0.41	0.09	N	0.06	0.02
Sandy loam	B	0.77	0.38	LN	1.89	0.16	N	0.41	0.09	B	0.06	0.02
Sandy clay loam	LN	0.58	0.34	LN	1.48	0.13	N	0.39	0.07	B	0.10	0.01
Loam	B	0.37	0.21	LN	1.56	0.11	N	0.43	0.10	B	0.08	0.01
Silt loam	LN	0.20	0.12	LN	1.41	0.12	N	0.45	0.08	B	0.07	0.01
Silt	N	0.18	0.06	N	1.38	0.04	N	0.46	0.11	B	0.04	0.01
Clay loam	LN	0.19	0.16	N	1.32	0.10	N	0.41	0.09	N	0.10	0.01
Silty clay loam	LN	0.11	0.06	LN	1.23	0.06	N	0.43	0.07	N	0.09	0.01
Sandy clay	LN	0.28	0.17	LN	1.28	0.08	N	0.38	0.05	B	0.10	0.01
Silty clay	LN	0.04	0.03	LN	1.16	0.05	N	0.36	0.07	N	0.07	0.02
Clay	LN	0.06	0.08	B	1.13	0.07	N	0.380	0.09	B	0.07	0.03

Note: B = beta; LN = lognormal; N = normal; μ = mean; σ = SD.

Appendix B – Risk Assessment Retrospective

The main hazards identified at the start of Michaelmas were:

(1) Inhalation of soil dust during transfer of soil samples
(2) Small voltage/current leakage
(3) Falling objects in the lab
(4) Water on floor causing slippery

These risks were present but to a much less severity than what was imagined while filling in the risk assessment. The risk that was considered relevant was (1). As fine sand was used, careless transfer of the sand could have indeed caused inhalation of soil dust. However, as the container available was rather small, the transfer of sand had to be done using shovels, which lowered the amount of sand transferred each time and minimised the amount of soil dust generated.

A risk that was encountered but not considered during the risk assessment stage was the risk of injury from improper lifting. As large amount of sand was needed and the balance was at a fixed location, there was a need to carry the sand back and forth with a bucket. To avoid injury from lifting overly heavy buckets of sand, smaller quantity of sand was shovelled into the bucket each time with more trips made.

Overall, the risk assessment predicted the encountered risks relatively well.

Appendix C – Covid-19 Disruption

There was one main disruption due to the Covid-19 pandemic.

In the project, a simple experiment was designed to verify the validity of the wedging factor as mentioned in Section 3. After one run, the container was scheduled to be used by other students, therefore it was intended that extra runs would be carried out as soon as the container becomes available again. However, the container only became available after the end of Lent term. I planned to carry out the remaining runs in the Easter break as my original plan was to stay in Cambridge over the Easter break. However, the pandemic then broke out and I had to go home in the first week of the Easter holiday, which means there was only one set of experimental data and it would be difficult to verify the analytical solution with the experiment. Thus, more focus was shifted onto using the Finite Element analysis in Section 4 to make up for the lack of data in the experiment.